



Validating the Generality of a Closed-Form Equation for Soil Water Isotherm

Shengmin Luo, A.M.ASCE¹; and Ning Lu, F.ASCE²

Abstract: Total soil water potential ψ_t is conventionally defined as the sum of matric potential ψ_m and osmotic potential ψ_o , i.e., $\psi_t = \psi_m + \psi_o$, when gravitational potential is ignored. Soil water isotherm (SWI) is the constitutive relationship between ψ_t and soil water content w, i.e., $\psi_t(w) = \psi_m(w) + \psi_o$, where $\psi_m(w)$ is called soil water retention curve (SWRC) or soil water characteristic curve. SWI and SWRC are arguably the two most important soil constitutive relationships because they govern virtually all phenomena in soil such as flow, stress and deformation, and biological activities. A closed-form SWI, recast from a generalized SWRC equation for adsorption and capillarity, is experimentally validated for its generality in representing SWI. Adsorption isotherms of 49 soils, covering all spectrum of soil types with plasticity index up to 185% and specific surface area up to 600 m²/g, are used to validate the SWI equation. It is shown that the SWI equation can nearly perfectly represent the isotherms of these soils with almost all of the coefficients of determination $R^2 \ge 0.99$, validating the generality of the SWI equation. Comparative analysis is also conducted by using two existing SWI equations, namely, the Brunauer–Emmett–Teller (BET) equation and the augmented BET (A-BET) equation. It is demonstrated that the SWI equation is superior to the BET and A-BET equations in representing soil–water interactions by adsorption and capillarity, and in the full relative humidity range. **DOI: 10.1061/(ASCE)GT.1943-5606.0002681.** © 2021 American Society of Civil Engineers.

Author keywords: Soil water retention curve (SWRC); Soil water characteristic curve; Soil water isotherm (SWI); Total soil water potential; Soil matric potential; Water sorption; Capillarity.

Introduction

Total soil water potential is the energy per unit mass of pore water in soil with respect to that of pure water under standard ambient air pressure and temperature (e.g., Iwata et al. 1995; Lu and Zhang 2019). As the result of an energy deficit between soil water and pure water, total soil water potential is designated as negative by convention. The total potential of soil water mainly consists of three forms of energy: gravitational, osmotic, and matric potentials (e.g., Hillel 1998; Lu and Likos 2004; Or et al. 2005; Osman 2013). Among these three potentials, matric potential is often dominant; thus, it can be practically considered as the total potential in most geotechnical engineering problems.

Intuitively, matric suction, a positive quantity defined as the negative of matric potential, is often used for soil under unsaturated conditions. When a soil—water system reaches equilibrium at a certain matric suction, the amount of water that can be retained by the soil is a definite value. The functional relationship between matric suction and soil water content is generally termed the soil water retention curve (SWRC). Considering that each soil has a unique mineralogical composition and pore-size distribution, SWRC is recognized as the constitutive function of a soil that fundamentally dictates basic soil properties such as swelling potential (e.g., McKeen 1992; Likos 2008), hydraulic conductivity

Note. This manuscript was submitted on March 28, 2021; approved on July 22, 2021; published online on September 16, 2021. Discussion period open until February 16, 2022; separate discussions must be submitted for individual papers. This paper is part of the *Journal of Geotechnical and Geoenvironmental Engineering*, © ASCE, ISSN 1090-0241.

(e.g., Mualem 1976; van Genuchten 1980), soil water density (e.g., Zhang and Lu 2018, 2020), soil water freezing (e.g., Koopmans and Miller 1966; Kurylyk and Watanabe 2013), and cavitation of soil water (Or and Tuller 2002; Frydman and Baker 2009; Lu 2019a). As such, characterizing the SWRC accurately is of vital importance for better understanding the behaviors of unsaturated soil (e.g., flow, stress and deformation, and biological activities).

Under natural and laboratory conditions, the matric suction of a soil can vary over 6 orders of magnitude from 0 kPa (commonly for saturation below water table) to 1.6×10^6 kPa (commonly for oven dryness) (Khorshidi and Lu 2017a, b). Two distinct physical mechanisms, i.e., adsorption and capillarity, are independently involved and are dominant at different stages of the soil water retention (SWR) processes (e.g., McQueen and Miller 1974; Tuller and Or 2005; Frydman and Baker 2009; Lu and Khorshidi 2015). Adsorption occurs at relatively high matric suction where soil water content is low, whereas capillarity starts to play more important roles at relatively low matric suction as the water content increases. The phenomenon of cavitation or capillary condensation bridges these two mechanisms. As a result of historically poor representation in adsorption, the most commonly used SWRC models such as the van Genuchten (VG) model (van Genuchten 1980) and the Fredlund and Xing (FX) model (Fredlund and Xing 1994) can usually fit the discrete SWR measurements well only for matric suction less than 1.5×10^3 kPa, and they have rarely been experimentally validated for matric suction greater than 1.5×10^5 kPa. Recently, Revil and Lu (2013) developed a first equation to explicitly incorporate both adsorption and capillarity into the definitions of SWR model parameters, which makes the model applicable to fit SWRC at full range of matric suction. Lu (2016) further improved the Revil and Lu (RL) model by introducing a cavitation function, enabling a drastic yet smooth transition on an SWRC from adsorptive- to capillary-dominated regimes.

¹Postdoctoral Fellow, Dept. of Civil and Environmental Engineering, Colorado School of Mines, Golden, CO 80401. ORCID: https://orcid.org/0000-0002-5433-6285. Email: shengminluo@mines.edu

²Professor, Dept. of Civil and Environmental Engineering, Colorado School of Mines, Golden, CO 80401 (corresponding author). ORCID: https://orcid.org/0000-0003-1753-129X. Email: ninglu@mines.edu

Over the past decade, a new hygrometer-based technique known as dynamic dew point or vapor sorption analyzer (VSA) (Likos et al. 2011; Lu 2020) has emerged as a feasible and time-saving tool for measuring high-resolution soil water isotherm (SWI), which unveils the relationship between relative humidity (i.e., partial vapor pressure) and pertinent soil water content equilibrated at a given temperature (i.e., isothermal condition). The relative humidity (RH) can be linked to the soil matric suction via Kelvin's equation (e.g., Lu and Likos 2004). Because SWI measured by VSA can typically offer several hundreds of SWR data points at the very high matric suction where adsorption is prevailing, it has been demonstrated as a promising way to characterize some fundamental soil properties such as specific surface area (SSA) (e.g., Akin and Likos 2014, 2016; Zhang and Lu 2019a) and cation exchange capacity (CEC) (Khorshidi and Lu 2017a, b).

In this study, a closed-form SWI equation recast from an SWRC model developed by Lu (2016) is adapted to model SWI data. The objectives are mainly threefold: (1) to adapt and validate the generality of the proposed SWI model for accurately representing the experimental data of all soil types; (2) to examine the applicability of the SWI model to the full RH range of measurements; and (3) to explicitly separate the SWI into two SWIs, i.e., the adsorptive SWI and capillary SWI.

Soil Water Retention Mechanisms and Models

Three distinct mechanisms for soil—water interactions, i.e., adsorption, capillarity, and cavitation/condensation, will serve as the theoretical basis for the proposed SWI model. As such, three relevant SWRC and SWI models, including Lu's (2016) generalized SWRC model, the Brunauer–Emmet–Teller (BET) equation (Brunauer et al. 1938), and the augmented BET equation (Zhang and Lu 2019a), will be briefly introduced in the following together with the illustrations of the three SWR mechanisms.

A Generalized Model for SWRC

Considering local energy equilibrium in soil water at any gravimetric water content w (or volumetric water content θ), recently synthesized soil sorptive potential (SSP) enables a unitary definition of matric suction $\psi(w)$ as follows (Lu 2019b; Zhang and Lu 2019b):

$$\psi(w) = u_{\rm a} - u_{\rm w}(x, w) - \psi_{\rm sorp}(x) \tag{1}$$

where $u_{\rm a}$ = pore air pressure (kPa); $u_{\rm w}(x,w)$ = local pore water pressure at a statistical distance x to the soil particle surface (kPa); and $\psi_{\rm sorp}(x)$ = SSP at the distance x (kPa).

For modeling SWRC, adsorption and capillarity can be described separately but be cast in one universal formula based on the preceding definition. In Lu's (2016) model, the total water content under an equilibrium matric suction is expressed as a mathematical sum of adsorptive and capillary components:

$$w(\psi) = w_a(\psi) + w_c(\psi) \tag{2}$$

where $w_a(\psi)$ = adsorbed water content (g/g); and $w_c(\psi)$ = capillary water content (g/g). The adsorptive water can be expressed as:

$$w_{\rm a}(\psi) = w_{\rm amax} \left\{ 1 - \left[\exp\left(\frac{\psi - \psi_{\rm max}}{\psi}\right) \right]^M \right\}$$
 (3)

where $w_{\rm amax}$ = gravimetric adsorption capacity (hereafter adsorption capacity) reflecting the maximum amount of water that can be retained by soil in the form of adsorption (g/g); $\psi_{\rm max}$ = maximum suction (kPa); and M = adsorption strength. The description of capillary

water content $w_{\rm c}(\psi)$ in Eq. (2) is adapted from the VG model, and a cumulative distribution function (CDF) of standard-normal distribution (probability varying between 0 and 1) is introduced to consider the cavitation or condensation of capillary water in soil:

$$w_{\rm c}(\psi) = \frac{1}{2} \left[1 - \text{erf}\left(\frac{\psi - \psi_{\rm c}}{\sqrt{2}\sigma_{\rm c}}\right) \right] [w_{\rm s} - w_{\rm a}(\psi)] [1 + (\psi/a)^n]^{1/n - 1}$$
(4)

where erf() = error function; $\psi_{\rm c}$ = mean cavitation suction (kPa); $\sigma_{\rm c}$ = standard deviation of the cavitation CDF (kPa); $w_{\rm s}$ = gravimetric water content at saturated state of soil (g/g); a = air-entry suction (kPa); and n = parameter of pore-size distribution. In Lu (2016), to simplify the fitting process, a fixed relationship of $\sigma_{\rm c} = 0.5 \psi_{\rm c}$ was suggested and used.

Fig. 1 shows a schematic of SWRC and its two constituent water retention curves. Three regimes can be identified on an SWRC in the order of decreasing suction or increasing water content, which are tightly adsorbed, adsorbed film, and capillary regimes (McQueen and Miller 1974; Lu and Likos 2004). For a soil with approximate oven dryness, the highest suction ψ_{\max} defined in the LU model ensures a maximum limit for matric suction, below which the adsorption occurs. Depending on mineralogy and cation type of the soil, this maximum matric suction has been found to vary greatly from 3.0×10^5 to 1.6×10^6 kPa (e.g., Jensen et al. 2015; Lu and Khorshidi 2015; Zhang et al. 2017). It can also be observed from Fig. 1 that the total water content is equal to the adsorptive water content in the suction range greater than approximately 10⁵ kPa, where water molecules are strongly bonded to the soil particle surface by short-ranged adsorptive forces (e.g., Derjaguin et al. 1987; Revil and Lu 2013). Specific

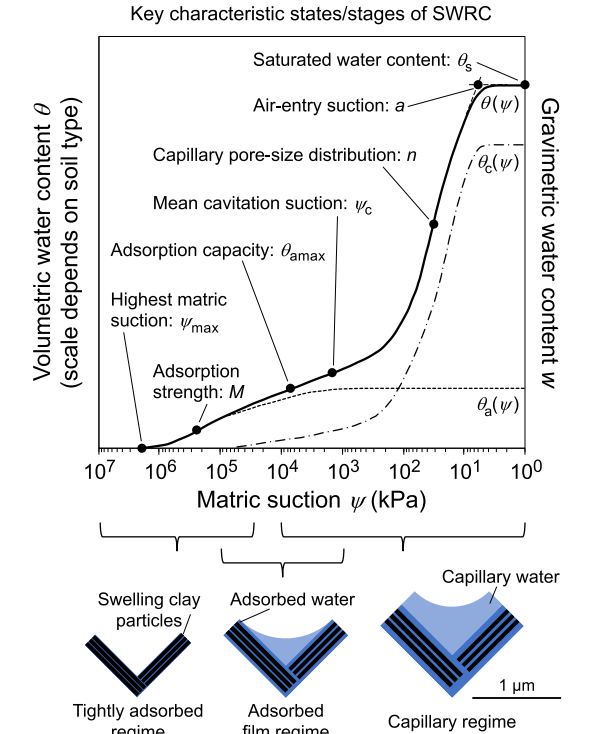


Fig. 1. Conceptual illustrations for soil water retention regimes, key characteristic states, and stages along an SWRC. (Adapted from Lu 2016.)

mechanisms contributing to water adsorption at this regime will be discussed in detail in the following sections.

In the range of matric suction lower than approximately 10^5 kPa, water vapor starts to condense in capillary form at the corners of micrometer-sized particles (Fig. 1), where an air–water interface is formed by connecting the water films absorbed on nearby particle surfaces. The adsorbed film regime is a transition state on an SWRC from the adsorptive- to the capillary-dominated regimes, and the capillary water content in this process is described in the LU model by using the mean cavitation suction ψ_c (i.e., reverse process of capillary condensation). In the adsorbed film regime, both adsorbed water and capillary water contribute to the increase of total water content. However, as the water content further increases, the adsorptive water content will eventually reach the adsorption capacity $w_{\rm amax}$, which is the maximum water content ascribed to the adsorptive forces. The strength to reach this maximum is controlled by the adsorption strength M.

When the matric suction is lower than approximately 10⁴ kPa, any further increase in total water content is solely attributed to capillary water. SWRC in the capillary regime is primarily governed by the pore-size distribution of the soil. For water content close to the saturated state, the transition from unsaturated to saturated state generally takes place smoothly but abruptly across

the air-entry suction a, which allows the soil to remain saturated at positive matric suction.

Previous SWI Models

As previously mentioned, RH and matric suction ψ are interconnected via Kelvin's equation (e.g., Lu and Likos 2004):

$$\psi = -\frac{RT}{v_{\rm w}} \ln \left(\text{RH} \right) \tag{5}$$

where R = universal gas constant (8.3145 × 10⁻³ kJ · mol⁻¹ · K⁻¹); T = temperature (K); and $v_{\rm w}$ = molar volume of water (1.8 × 10⁻⁵ m³/mol at 100 kPa and 25°C). Based on the preceding equation, the isotherm represents an SWRC at medium to high suction range [Figs. 2(a and b)], where three types of adsorption have been identified and quantified, i.e., cation hydration, surface hydration, and hydration of interlayer complexes (e.g., Khorshidi et al. 2016; Zhang and Lu 2018).

The concept of SSP clearly demonstrates that these adsorption mechanisms are all electromagnetic in nature (Lu and Zhang 2019). Water molecules with strong polarity are attracted to the soil

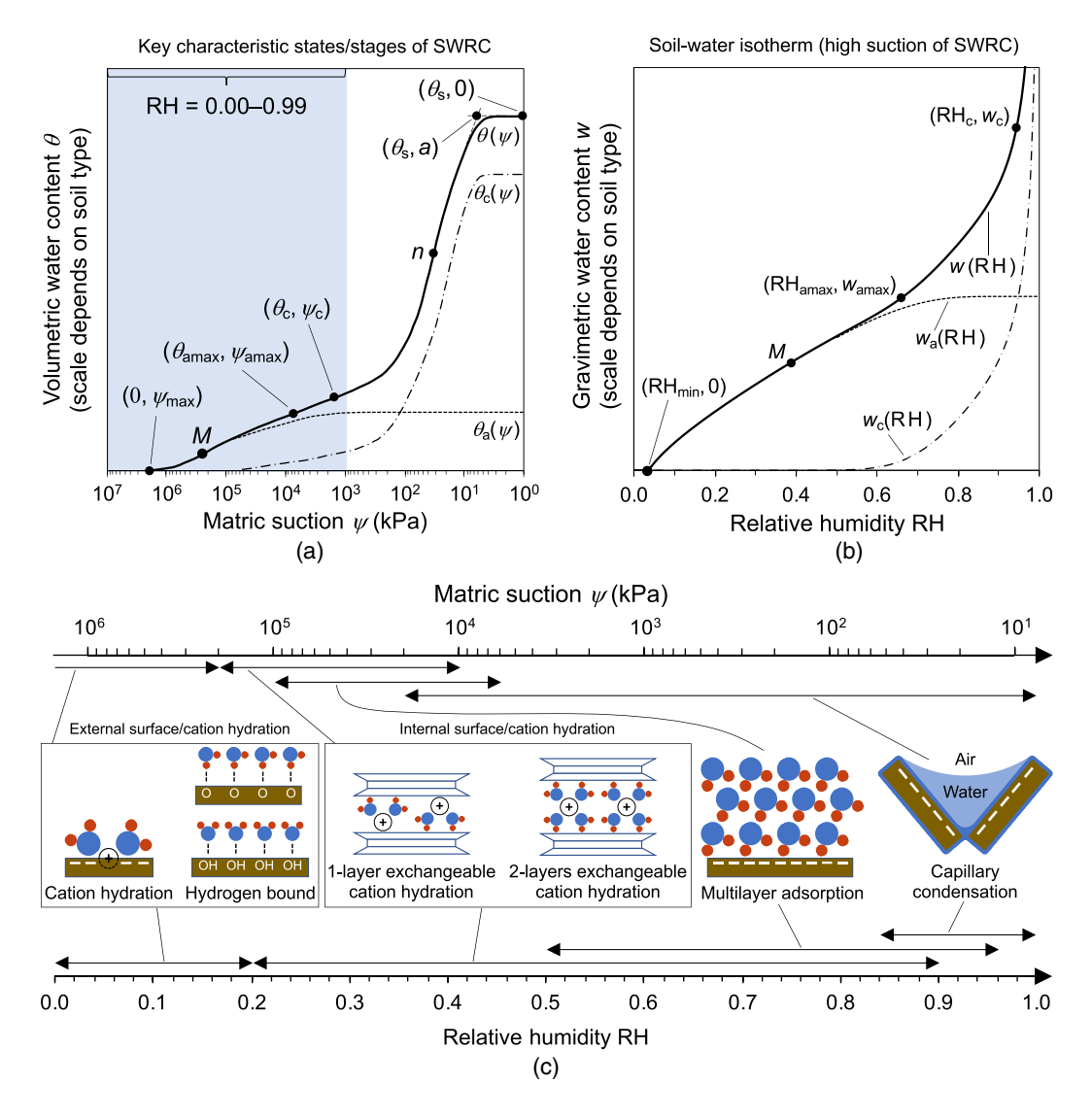


Fig. 2. Illustrations of physicochemical mechanisms for soil—water interactions at different ranges of matric suction and relative humidity. [Part (c) adapted from Lu and Zhang 2020.]

particle surface or interlamellar surface by various intermolecular forces. Fig. 2(c) illustrates the range of different adsorptive mechanisms in terms of both matric suction and RH. The wetting of an initially dry soil commences with hydration of cation retained on the external surface by Coulomb electric attractive force at the atomic scale (Khorshidi et al. 2016). Hydrogen bonds between oxygen/hydroxyl anions exposed on the external surface and water molecules are then formed by van der Waals attraction (Zhang and Lu 2019a), which is the intermolecular force also responsible for the subsequent multilayer adsorption. For expansive soils, the van der Waals attraction and Coulomb attraction between clay's interlamellar layers would produce an energy barrier that retards the water hydration of interlayer complexes (i.e., interlayer exchangeable cation and surface).

The Brunauer–Emmet–Teller (BET) equation (Brunauer et al. 1938) is a commonly used SWI model to describe the multilayer adsorption of water molecules on soil particle surface. The sorption isotherm of a soil can be fitted by the BET equation as follows:

$$w = \frac{w_{\rm m}cRH}{(1 - RH)(1 - RH + cRH)}$$
 (6)

where w = gravimetric water content (g/g); RH = relative humidity; $w_{\rm m}$ = monolayer water content (g/g); and c = constant related to the enthalpy of adsorption.

However, it has long been recognized that the BET equation is not applicable to the entire RH range for soil but merely functions between about 0.05 and 0.35 (e.g., Mooney et al. 1952; Yamanaka et al. 1990), mainly due to the following two reasons: (1) assuming a homogeneous adsorbent surface in the original theory; and (2) neglecting the long-ranged capillary mechanism that depends on the pore structure. To overcome the first unrealistic assumption, Zhang and Lu (2019a) proposed an augmented BET (A-BET) equation for soil to separate the heterogeneous adsorption process into two subprocesses with distinct ranges of matric suction (Fig. 2): external and internal surface adsorptions. Assuming that each of these two components can be individually described by the original BET equation, the total adsorbed water content w(RH) is thus described by the following equation:

$$\begin{split} w(\text{RH}) = & \frac{w_{\text{m-ext}} c_{\text{ext}} \text{RH}}{(1 - \text{RH})(1 - \text{RH} + c_{\text{ext}} \text{RH})} \\ & + \frac{w_{\text{m-int}} c_{\text{int}} (\text{RH} - \text{RH}_0)}{[1 - (\text{RH} - \text{RH}_0)][1 - (\text{RH} - \text{RH}_0) + c_{\text{int}} (\text{RH} - \text{RH}_0)]} \end{split}$$

where $w_{\rm m-ext}$ and $w_{\rm m-int}$ = monolayer water contents adsorbed on the external and internal surfaces, respectively (g/g); $c_{\rm m-ext}$ and $c_{\rm m-int}$ = constants related to the enthalpy of adsorption on external and internal surfaces, respectively; and RH₀ = relative humidity where the energy barrier is overcome and adsorption on the internal surface initiates. The onset RH of capillary condensation, which constrains the maximum applied range of the A-BET equation, is identified based on the sharp decline in local c (enthalpy of adsorption) value (Pomonis et al. 2004; Zhang and Lu 2019a).

A Generalized SWI Model

Formulation of the Proposed SWI Model

Given that the LU model was originally developed to fit the entire SWRC, especially outperforming the other SWRC models in high suction range (Lu 2016; Dong and Lu 2020; Zhang and Lu 2020;

Zhou and Lu 2021b), a closed-form equation is recast and adapted for SWI over the full range of RH by preserving the general expressions of the LU model. This is first done by casting Eqs. (2)–(4) in terms of RH through Kelvin's Eq. (5):

$$w(RH) = w_a(RH) + w_c(RH) \tag{8}$$

$$w_{\rm a}({\rm RH}) = w_{\rm amax} \left\{ 1 - \left[\exp\left(1 - \frac{\ln({\rm RH}_{\rm min})}{\ln({\rm RH})} \right) \right]^M \right\} \qquad (9)$$

$$\begin{split} w_{\rm c}({\rm RH}) &= \frac{1}{2} \left[1 - {\rm erf} \left(\frac{{\rm RH} - \mu_{\rm RH}}{\sqrt{2} \sigma_{\rm RH}} \right) \right] [w_{\rm s} - w_{\rm a}({\rm RH})] \\ &\times \left\{ 1 + \left[\frac{RT \ln({\rm RH})}{v_{\rm w} a} \right]^n \right\}^{1/n - 1} \end{split} \tag{10}$$

where $w_{\rm a}({\rm RH})$ and $w_{\rm c}({\rm RH})$ = adsorptive and capillary isotherms, respectively; RH_{min} = minimum relative humidity corresponding to the maximum matric suction; and $\mu_{\rm RH}$ and $\sigma_{\rm RH}$ = mean and standard deviation of the cavitation function, respectively, defined in terms of relative humidity.

The major adaptation in the proposed SWI equations comes from the cavitation function inside the first square brackets of Eq. (10), where a physically realistic CDF of a skew-normal distribution, instead of a standard-normal distribution, is used:

$$CDF(RH) = \Phi\left(\frac{RH - \xi}{\omega}\right) + 2T\left(\frac{RH - \xi}{\omega}, \alpha\right)$$
 (11)

The new cavitation function consists of two individual functions, i.e., CDF of a normal distribution $\Phi()$ and Owen's T function T(), and is defined by three cavitation parameters: onset relative humidity ξ , cavitation humidity range ω , and CDF shape parameter α .

Considering that the phenomenon of soil–water cavitation mostly occurs in the capillary regime with RH greater than 0.8 (e.g., Tuller and Or 2005), Fig. 3 illustrates the CDF of four skewnormal distributions with the same ξ and ω of 1.0 and 0.1 but different α values varying from -5 to 0, showing that normal distribution is a special case of skew-normal distribution with $\alpha=0$. The physical basis for using a skew-normal distribution to represent the cavitation function is to avoid the unrealistically low CDF value (i.e., 0.5) of standard-normal distribution when the onset relative humidity ξ is close to 1.0 (Fig. 3). In other words, the water

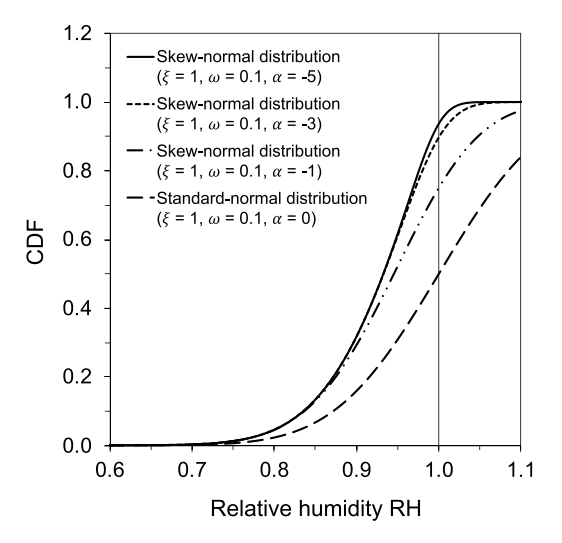


Fig. 3. Illustration of cavitation distribution functions of skew- and standard-normal distributions.

contents near saturation can be significantly underestimated without using a new cavitation function. Experimental evidence indicates that the probability of acoustic cavitation in water does not always follow a standard-normal distribution but exhibits certain skewness (Herbert et al. 2006). Fig. 3 also demonstrates that the CDF will not change significantly once the α value is reduced to -5. As such, Eq. (11) is proposed, and a constant value of -5 is used for the CDF shape parameter α in this study.

To minimize uncertainties due to multiple-parameter identifications, further simplifications can be made to the proposed SWI equation. For most soils, the air-entry suction a is generally less than 10 kPa (e.g., Lu 2016), which corresponds to RH greater than 0.99. Since SWI data from the VSA techniques are generally available at RH less than 0.95, the parameter a is set to be 1 kPa, i.e., RH = 0.99999. Moreover, a simplified relationship (M = 1 - 1/n) similar to that commonly assumed in using the VG model is used for adsorption strength M and pore-size distribution parameter n, due to their strong correlation revealed by a preliminary sensitivity study. Substituting these adaptations and simplifications into Eqs. (9) and (10) leads to the final equations for the proposed SWI:

$$w_{\rm a}({\rm RH}) = w_{\rm amax} \left\{ 1 - \left[\exp \left(1 - \frac{\ln({\rm RH}_{\rm min})}{\ln({\rm RH})} \right) \right]^{1 - 1/n} \right\} \quad (12)$$

$$\begin{split} w_{\rm c}({\rm RH}) &= \left[\Phi\!\left(\!\frac{{\rm RH}-\xi}{\omega}\!\right) + 2{\rm T}\!\left(\!\frac{{\rm RH}-\xi}{\omega}, -5\right)\right]\!\left[w_{\rm s} - w_{\rm a}({\rm RH})\right] \\ &\times \left\{1 + \left[\!\frac{RT\ln({\rm RH})}{v_{\rm w}}\!\right]^n\right\}^{1/n-1} \end{split} \tag{13}$$

Model Fitting Procedure

The proposed SWI model, i.e., Eqs. (8), (12), and (13), is completely controlled by six parameters, namely the minimum relative humidity RH_{min} , adsorption capacity w_{amax} , onset of cavitation humidity ξ , extent of cavitation humidity ω , pore-size distribution n, and saturated water content w_s . Generally speaking, the saturated water content w_s is directly linked to a soil's porosity ϕ and specific gravity G_s by

$$w_{\rm s} = \frac{\phi}{G_{\rm s}(1-\phi)} \tag{14}$$

A constant value $G_{\rm s}$ of 2.65 is assumed if the measurement is not available. Similarly, a porosity ϕ of 0.5 is assigned to soils when it is not reported.

Because the saturated water content w_s is known for each soil, the remaining five parameters are determined iteratively by using an R package developed for nonlinear regression, *minpack.lm* (Elzhov et al. 2016). According to the classical nucleation theory for water cavitation (e.g., Caupin and Herbert 2006; Debenedetti 1996), capillary water under negative pressure (i.e., lower than the pore air pressure) is unlikely to exist at matric suction higher than 1.9×10^5 kPa (equivalent to RH = 0.25). Therefore, capillary water [Eq. (13)] at RH lower than 0.25 is manually set as zero for each iteration. Also, to minimize the effect of parameter initialization on the fitting output, the five fitted parameters of each soil are randomly initialized 100 times to identify the best set of model parameters with the highest coefficient of determination, R^2 .

SWI Database for Model Validation

Experimental isotherm data for a suite of 49 soils from the literature, i.e., 20 from Akin and Likos (2014), 17 from Khorshidi et al.

(2017), and 12 from Zhou and Lu (2021a), are employed to assess the performance of the proposed SWI model. The basic soil physical and geotechnical index properties of these soils are summarized in Table 1. According to the Atterberg limits (ASTM 2017) and the Unified Soil Classification System (USCS), these soils cover a wide variety of soil types from sandy soil to swelling clay with plasticity index (PI) varying considerably from 4 to 185. The SSA and CEC range up to 600 m²/g and 169.0 cmol/kg, respectively, giving a full coverage of swelling potential from low to medium, to high, and to very high (Table 1). In addition, both natural soils and mixed clays are used to examine the generality of the proposed SWI model, and the latter includes cation-exchanged bentonites as well as kaolinite and bentonite clay mixtures.

Based on the soil type and mineralogy, these soils are grouped into six categories (Table 1): sandy soil (I), silty soil (II), nonswelling clay (III), swelling clay (IV), cation-exchanged bentonite (V), and clay mixture (VI). Some of the listed soils were collected from the same general location but with different soil compositions, and some isotherms of the same soil were measured independently by different investigators. The water vapor isotherms were measured by the VSA (Meter Group, Pullman, Washington) at room temperature (~25°C). A complete wetting-drying loop of isotherm typically includes approximately 200 discrete data points. For most soils, the adsorption isotherms (wetting path) were used to fit the model parameters, except for the kaolinite/bentonite mixtures for which only the desorption isotherms (drying path) were available.

SWI Model Performance

The model performance will be assessed in three aspects: fitness to model the measured SWI data of various soil types, capability to separate adsorptive SWI and capillary SWI, and comparison with other SWI models. The isotherms of 44 different soils will be visually and fully exhibited herein. To inclusively demonstrate the generality of the proposed SWI model, all of these isotherms will not be displayed twice.

Overall Fitting Assessment

The best-fit parameters and the corresponding coefficient of determination R^2 for all soils are listed in Table 2. It can be observed that the proposed SWI equation can nearly perfectly model the isotherm data for all types of soils, as evidenced by the very high R^2 (all greater than 0.99). The only two exceptions are Kaifeng sand $(R^2=0.91)$ and commercial kaolin $(R^2=0.72)$, whose isotherm data fluctuate at RH < 0.1 as the VSA approaches its resolution in water content measurement.

The predicted adsorption capacity, as summarized in Table 2, ranges from 0.01 g/g for sandy and silty soils (e.g., Kaifeng sand and Heifangtai silt) as well as up to 0.2 g/g for swelling clays (e.g., Wyoming bentonite I and Denver bentonite II). Among them, the values identified for Georgia kaolinite and Wyoming bentonite are 0.02 g/g and 0.2 g/g. These two adsorption capacities are very close to the water contents of two clays respectively corresponding to mono-layer hydration (0.01 g/g) and three-layers hydration (0.2 g/g) reported in the literature (Keren and Shainberg 1979; Likos and Lu 2002), indicating the accuracy of the SWI model for parameter identification. Furthermore, based on the available adsorption studies in the literature (Dong and Lu 2016, 2020; Lu 2016; Zhou and Lu 2021b), predictions of the adsorption capacity in terms of SWRC are also gathered independently for 11 of the studied soils, and the volumetric water contents are converted to the gravimetric ones by using Eq. (14). Comparisons of the

Table 1. Geotechnical properties of the studied 49 soils

Group No.	Soil name and reference	LL (%)	PL (%)	PI	USCS	Total SSA (m ² /g) ^{a,b}	CEC (cmol/kg) ^{b,c}	Swelling potential ^d
I	Balt silt II ^e	28	23	5	SM	47	24.0	Low
	Commercial kaolin ^b	42	35	7	ML	21	0.4	High
	Hopi silt I ^e	26	19	7	SC-SM	61	20.0	Low
	Albany red sandy clay ^f	30	16	14	SC	55	7.6	Medium
	New Orleans sandy clay ^f	30	12	18	CL sandy	22	8.0	Medium
	Kaifeng sand ^b	37	5	32	SC	25	1.6	_
П	Bonny silt ^e	25	21	4	ML	67	21.0	Low
	Heifangtai silt ^e	26	21	5	ML	28	7.0	Low
	Balt silt I ^e	26	19	7	CL-ML	54	20.0	Low
	Iowa silt ^e	33	24	9	ML	62	22.0	Medium
	Alb1 silty clay	28	17	11	CL	41	8.5	Low
	Zhengzhou silt ^b	26	15	11	CL	26	5.0	Low
	Atlanta, Georgia silt ^f	50	36	14	MH	_	_	Medium
	Denver silty clay ^f	49	23	26	CH	_	_	High
	Hopi silt II ^e	_	_	_	ML	57	22.0	_
III	Mon 2 clay ^f	31	17	14	CL	56	15.2	Medium
	Sanmenxia silty clayb	35	19	16	CL	110	14.9	Medium
	Sacramento clay ^f	39	22	17	CL	202	27.8	Medium
	Georgia kaolinite ^e	44	26	18	CL	26	9.0	High
	KF1 clay ^f	42	23	19	CL	189	35.6	High
	Denver claystone II ^e	44	23	21	CL	67	35.0	High
	Jingmen brown soil ^b	42	21	21	CL	144	25.4	High
	Wuhan clay ^b	40	18	22	CL	94	15.4	High
	Denver claystone I ^b	46	23	23	CL	90	16.0	High
	Xinyang clay ^b	42	19	23	CL	114	20.6	High
	KF2 clay ^f	41	15	26	CL	148	23.4	High
	Kamm clay ^f	49	21	28	CL	134	26.3	High
	Wcs Andrew clay ^f	50	18	32	CH	83	17.6	High
IV	Alb2 clay ^f	36	14	22	CL	24	8.1	Medium
	Houston brown clay ^f	41	16	25	CH	157	32.2	High
	Jingmen yellowish-brown soil ^b	63	26	37	CH	251	30.9	Very high
	Denver bentonite I ^b	104	48	56	MH	566	97.6	Very high
	Denver bentonite II ^e	118	45	73	CH	591	169.0	Very high
	Ningming expansive soil ^b	165	38	127	CH	375	50.8	Very high
	Wyoming bentonite II ^e	485	353	132	CH	594	75.0	Very high
	Wyoming bentonite I ^e	218	33	185	СН	600	62.1	Very high
V	Na ⁺ /Ca ²⁺ -bentonite ^e	_	_	_	_	_	74.0	_
	Na ⁺ -bentonite ^e	_	_	_	_	_	_	_
	Ca ²⁺ -bentonite ^e	_	_	_	_	547	_	_
	Mg ²⁺ -bentonite ^e	_	_	_	_	453	_	_
	Li ⁺ -bentonite ^e	_	_	_	_		_	_
	K ⁺ -bentonite ^c	_	_	_	_	196	_	_
VI	100%kaolinite ^f	_	_	_	_	_	_	_
	80%kaolinite/20%bentonite ^f	_	_	_	_	_	_	_
	50%kaolinite/50%bentonite ^f	_	_	_	_	_	_	_
	30%kaolinite/70%bentonite ^f	_	_	_	_	_	_	_
	20%kaolinite/80%bentonite ^f	_	_	_	_	_	_	_
	10%kaolinite/90%bentonite ^f	_	_	_	_	_	_	_
	100% bentonite ^f							

Note: PI = plasticity index; LL = liquid limit; PL = plastic limit; and USCS = unified soil classification system.

adsorption capacity between the isotherm with the proposed model and the SWRC with Lu's (2016) model indicate that the adsorption capacity predicted from this study and the literature are statistically similar and well correlated ($R^2=0.91$), as shown in Fig. 4. For some soils, the adsorption capacity from the SWRC modeling may seem to be slightly higher than that from the SWI, i.e., data

points located above the line of perfect match. This can potentially be attributed to the effect of hysteresis if the SWR data were measured from the drying path.

Furthermore, the model performance for the fitness to the isotherm data is visually exhibited in Fig. 5, which samples 20 soils representing the four main categories of sandy soil, silty soil,

^aLu and Zhang (2020).

^bZhou and Lu (2021b).

^cAkin and Likos (2016).

^dChen (1988).

^eKhorshidi et al. (2017).

fAkin and Likos (2014).

Table 2. Results of the fitted parameters for the SWI model

Group no.	Soil name	G_{s}	ϕ	RH_{min}	$w_{\rm amax}~({\rm g/g})$	n	ξ	ω	R^2
I	Balt silt II	2.65	0.50	0.00492	0.02	1.30	1.00	0.22	1.00
	Commercial kaolin	2.75	0.50	0.00001	0.01	1.47	1.00	0.20	0.72
	Hopi silt I	2.65	0.50	0.00011	0.03	1.29	1.00	0.37	1.00
	Albany red sandy clay	2.65	0.50	0.00001	0.03	1.15	0.98	0.09	0.99
	New Orleans sandy clay	2.65	0.50	0.02185	0.01	1.27	1.00	0.15	1.00
	Kaifeng sand	2.68	0.40	0.00001	0.01	1.44	1.00	0.62	0.91
П	Bonny silt	2.65	0.50	0.00033	0.02	1.28	1.00	0.35	1.00
	Heifangtai silt	2.65	0.50	0.00001	0.01	1.40	0.95	0.42	1.00
	Balt silt I	2.65	0.50	0.00157	0.02	1.30	1.00	0.26	1.00
	Iowa silt	2.65	0.50	0.00205	0.03	1.27	1.00	0.21	1.00
	Alb1 silty clay	2.65	0.50	0.00861	0.03	1.11	1.00	0.07	1.00
	Zhengzhou silt	2.70	0.50	0.00026	0.01	1.35	1.00	0.46	0.99
	Atlanta, Georgia silt	2.65	0.50	0.00120	0.03	1.17	1.00	0.12	1.00
	Denver silty clay	2.65	0.50	0.01391	0.04	1.27	0.95	0.12	1.00
	Hopi silt II	2.65	0.50	0.00015	0.02	1.27	1.00	0.34	1.00
Ш	Mon 2 clay	2.65	0.50	0.00219	0.03	1.28	1.00	0.25	1.00
	Sanmenxia silty clay	2.72	0.50	0.00642	0.03	1.25	1.00	0.18	1.00
	Sacramento clay	2.65	0.50	0.01457	0.06	1.24	0.95	0.12	1.00
	Georgia kaolinite	2.65	0.57	0.03071	0.02	1.24	1.00	0.10	1.00
	KF1 clay	2.65	0.50	0.00909	0.08	1.22	0.94	0.10	1.00
	Denver claystone II	2.65	0.50	0.00383	0.04	1.22	1.00	0.20	1.00
	Jingmen brown soil	2.72	0.50	0.00030	0.05	1.18	1.00	0.20	1.00
	Wuhan clay	2.73	0.50	0.00473	0.03	1.20	1.00	0.16	1.00
	Denver claystone I	2.72	0.50	0.00135	0.04	1.24	1.00	0.19	1.00
	Xinyang clay	2.72	0.50	0.00033	0.05	1.20	1.00	0.21	1.00
	KF2 clay	2.65	0.50	0.01727	0.04	1.29	0.94	0.12	1.00
	Kamm clay	2.65	0.50	0.00001	0.05	1.24	0.95	0.12	0.99
	Wes Andrew clay	2.65	0.50	0.00035	0.04	1.20	1.00	0.20	1.00
IV	Alb2 clay	2.65	0.50	0.03220	0.03	1.10	1.00	0.06	1.00
IV	Houston brown clay	2.65	0.50	0.01603	0.04	1.10	0.95	0.13	1.00
		2.75	0.50	0.01003	0.04	1.14	1.00	0.15	1.00
	Jingmen yellowish-brown soil								
	Denver bentonite I	2.73	0.65	0.00011	0.16	1.20	1.00	0.15	1.00
	Denver bentonite II	2.65	0.65	0.00011	0.18	1.17	1.00	0.16	1.00
	Ningming expansive soil	2.73	0.70	0.03240	0.16	1.11	1.00	0.04	1.00
	Wyoming bentonite II Wyoming bentonite I	2.65 2.70	0.70 0.70	0.05193 0.03750	0.19 0.20	1.12 1.09	1.00 0.99	0.04 0.02	1.00 0.99
V									
	Na^+/Ca^{2+} -bentonite	2.65	0.70	0.00853	0.18	1.09	1.00	0.04	1.00
	Na ⁺ -bentonite	2.65	0.70	0.02945	0.18	1.11	1.00	0.04	1.00
	Ca^{2+} -bentonite	2.65	0.70	0.00290	0.15	1.29	0.94	0.09	0.99
	Mg ²⁺ -bentonite	2.65	0.70	0.00076	0.13	1.23	0.99	0.15	1.00
	Li ⁺ -bentonite K ⁺ -bentonite	2.65 2.65	0.70 0.70	0.00001 0.03412	0.19 0.08	1.05 1.25	1.00 0.99	0.06 0.08	0.99 1.00
VI	100% kaolinite	2.65	0.57	0.04570	0.01	1.33	1.00	0.12	1.00
	80% kaolinite/20% bentonite	2.65	0.60	0.03340	0.03	1.26	1.00	0.12	1.00
	50% kaolinite/50% bentonite	2.65	0.64	0.04090	0.08	1.20	1.00	0.07	1.00
	30% kaolinite/70% bentonite	2.65	0.66	0.03740	0.11	1.19	1.00	0.07	1.00
	20% kaolinite/80% bentonite	2.65	0.67	0.03150	0.12	1.17	1.00	0.07	1.00
	10% kaolinite/90% bentonite	2.65	0.69	0.03220	0.14	1.16	1.00	0.06	1.00
	100% bentonite	2.65	0.70	0.03580	0.15	1.18	0.99	0.07	1.00

nonswelling clay, and swelling clay (i.e., Groups I–IV in Table 1). The ranges of maximum water content of the measured isotherm data in these four plots are in an increasing order: 0.01–0.05 [Fig. 5(a)], 0.02–0.08 [Fig. 5(b)], 0.05–0.12 [Fig. 5(c)], and 0.09–0.23 [Fig. 5(d)]. As demonstrated, the fitted SWI closely follows the experimental data points (about 100 for each isotherm) over the entire measured range of RH from 0.03 to 0.95. The coefficients of determination R^2 are very high, nearly all equal to 1.00. In general, the isotherms show a clear increasing trend in water content as a soil becomes finer and finer. For instance, Denver bentonite I, with an SSA of $566 \text{ m}^2/\text{g}$ and a CEC of 97.6 cmol/kg, has higher water

content in the initial tightly adsorbed regime (RH < 0.5) than other soils with less SSA and CEC. A soil's ability to adsorb water becomes weaker and weaker as the soil becomes coarser and coarser like those sandy and silty soils with low PIs [e.g., commercial kaolin, Kaifeng sand, Heifangtai silt, and Zhengzhou silt shown in Figs. 5(a and b)]. The low adsorptive water contents for these soils are attributable to the fact that their SWR mechanism is mostly governed by the capillarity. Thus, a relatively flat shape can be observed on the isotherms of these soils in the RH range of 0.03-0.90, followed by a drastic increase at RH > 0.90 due to the onset of capillary water retention mechanism [Figs. 5(a and b)].

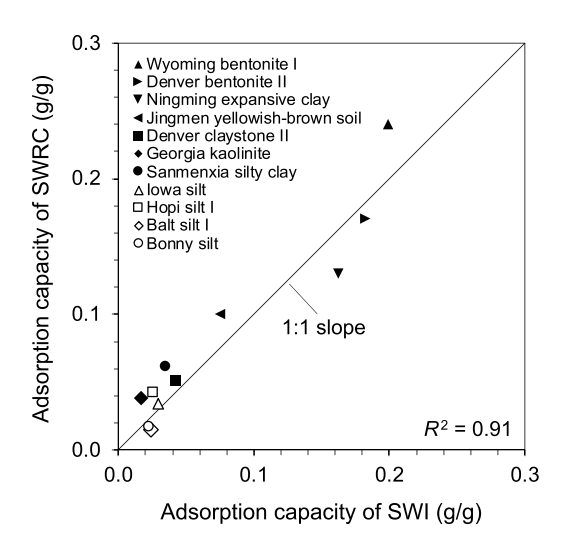


Fig. 4. Comparisons of adsorption capacity determined respectively using SWI and SWRC for 11 soils.

Therefore, it is concluded that the proposed SWI model can be used to accurately represent soil water isotherms of all types of soil at the full range of RH, ascribing to the explicit conceptualization and quantification of adsorptive, capillary, and cavitation mechanisms

by providing clear physical interpretation for each model parameter.

Separation of Adsorptive and Capillary Isotherms

The proposed SWI model is further assessed by examining both the fitted isotherm and its constituent adsorptive and capillary isotherms from several aspects, including for (1) a variety of soil types; (2) cation-exchanged bentonites; and (3) kaolinite-bentonite clay mixtures. Fig. 6 first shows the model fitting for six selective soils from Groups I–IV, including two silty soils [Figs. 6(a and b)] and four widely studied clays with diverse swelling potentials [Figs. 6(c-f)]. As shown, the proposed SWI model performs well for fitting these isotherms, with a minimum R^2 value of 0.99. The total water content is physically decomposed into the adsorptive and capillary components. The adsorptive water exists over the entire range of RH, but the capillary water can only exist at high RH. For instance, the capillary isotherm of Bonny silt [Fig. 6(a)] is only present when RH is greater than approximately 0.37, before which the fitted isotherm is totally attributed to the adsorptive isotherm. A similar limit of approximately 0.39 can be found for Hopi silt II [Fig. 6(b)]. Whereas the capillary isotherms of the four clays [Figs. 6(c-f)] do not occur until RH is approximately equal to 0.6. This capillary onset can even shift to as high as 0.93 for clayey soil, such as that observed for Wyoming bentonite I [Fig. 6(e)]. Such difference in the onset of capillary condensation is largely caused

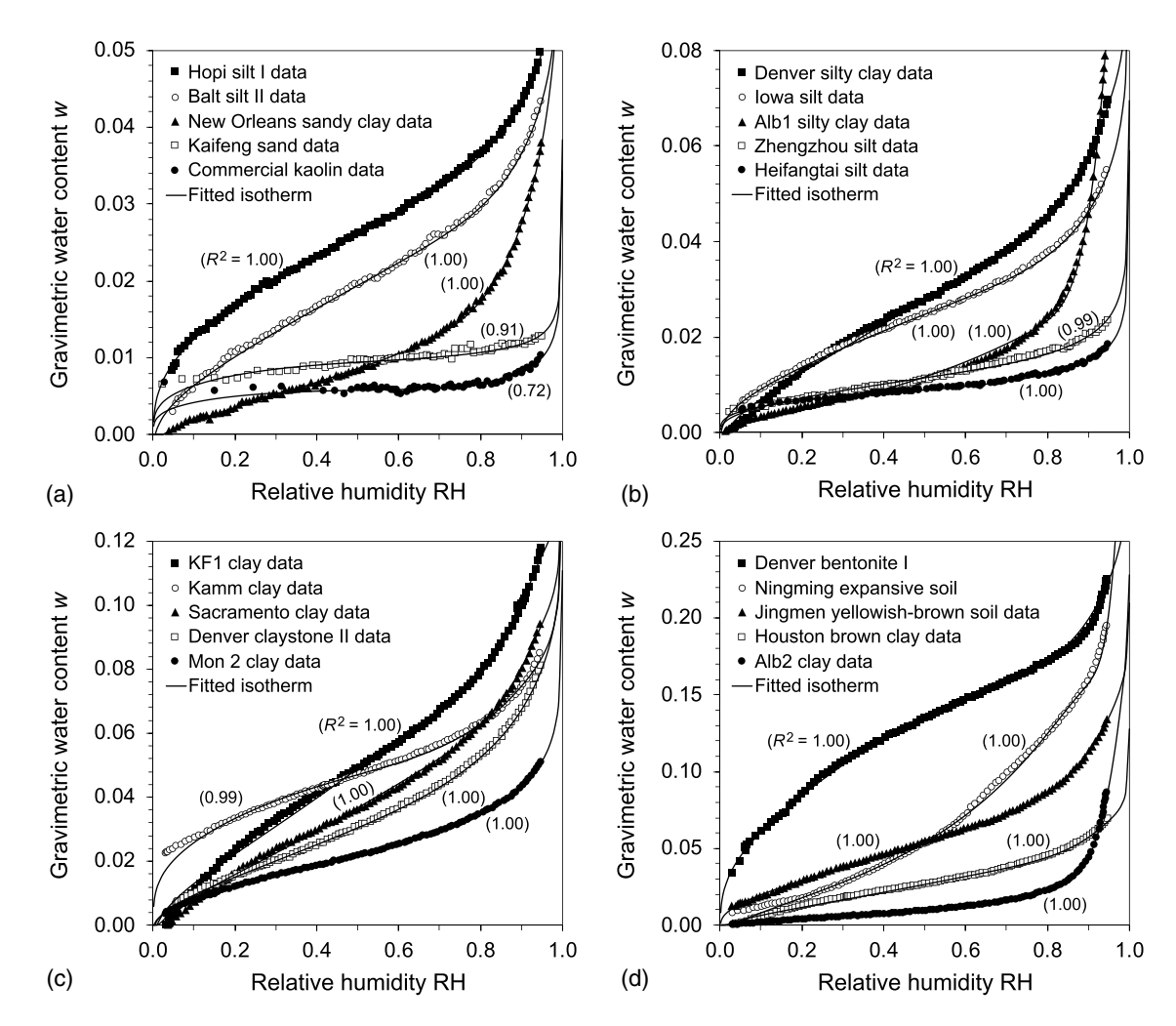


Fig. 5. Fitted isotherms for four types of soil: (a) sandy soil; (b) silty soil; (c) nonswelling clay; and (d) swelling clays.

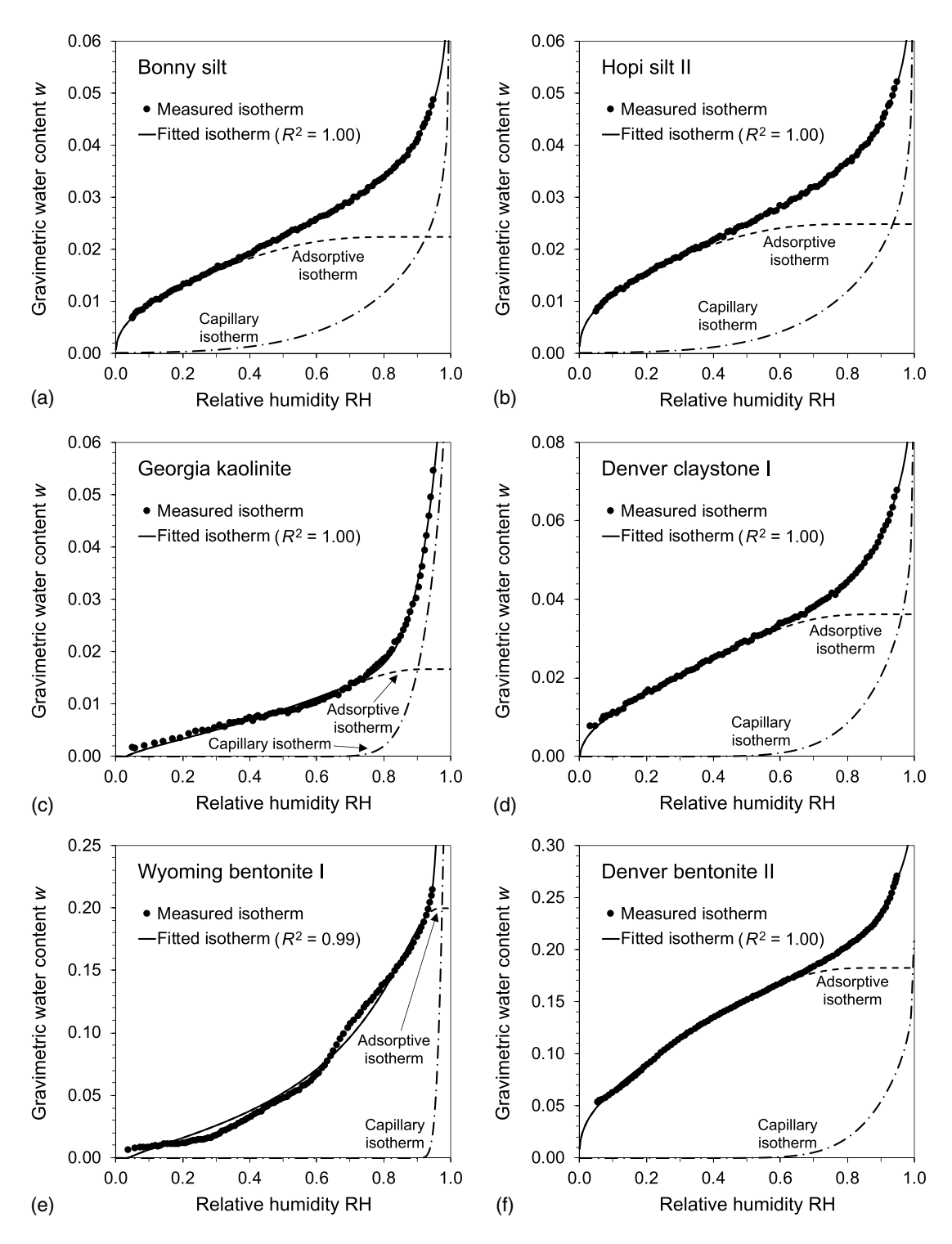


Fig. 6. Fitted isotherms and separated adsorptive and capillary isotherms for different types of soils.

by the discrepancy in soil particle sizes and ability to retain water in the form of adsorption, because capillary isotherm often appears while the adsorptive isotherm gradually approaches the adsorption capacity $w_{\rm amax}$ (i.e., the total adsorptive water content). In general, the lower a soil's sorptive potential (i.e., combined effect of van der Waals, electric double layer, and exchangeable cation) is, the higher adsorption capacity can be expected. As shown in Fig. 6 from (a) to (f), the predicted adsorption capacity gradually increases as the adsorption on the soil particle surface becomes stronger from silty soils to bentonite clays, qualitatively confirming the capability

of the proposed SWI to reflect soil's adsorption capacity in different soil types.

The fitted SWI results of a natural Na $^+$ /Ca $^{2+}$ -bentonite and its other cation-exchanged forms are illustrated in Fig. 7, giving a comparison of water sorption behavior among soils with the same mineralogy but different types and valencies of exchangeable cation. As shown, the proposed model can well represent the isotherms of six bentonites, showing all R^2 values greater than or equal to 0.99. Fig. 7 also demonstrates that the types of exchangeable cation can impose a significant effect on the water sorption behaviors of

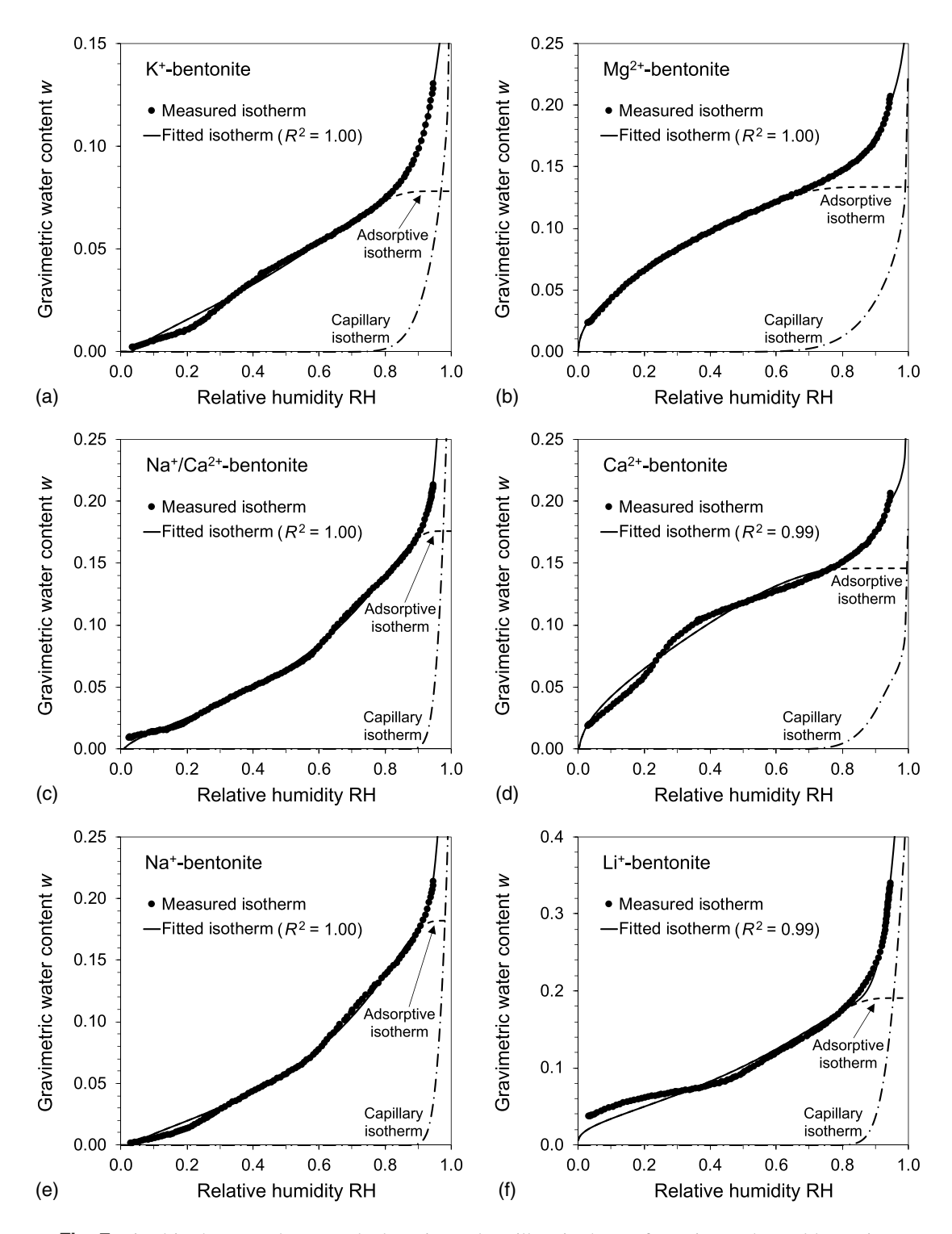


Fig. 7. Fitted isotherms and separated adsorptive and capillary isotherms for cation-exchanged bentonites.

swelling bentonite clays, consistent with the findings in the literature (e.g., Villar and Lloret 2008; Schanz and Tripathy 2009; Du et al. 2021). The water content at 0.95 RH varies from 0.22 for the untreated Na $^+$ /Ca $^{2+}$ -bentonite to a much lower value of 0.13 for K $^+$ -bentonite and to a much higher value of 0.34 for Li $^+$ -bentonite. The adsorption capacities identified for the five mono-cation bentonites are 0.08 (K $^+$), 0.18 (Na $^+$), 0.19 (Li $^+$), 0.15 (Ca $^{2+}$), and 0.13 (Mg $^{2+}$). In general, the hydration energy of exchangeable cations can have an appreciable effect on the amount of water adsorbed by the bentonite clay (e.g., Montes-H

et al. 2003; Akin and Likos 2014). According to Bohn et al. (2001), the enthalpy of hydration (i.e., hydration heat) for the aforementioned five cation types are K⁺ (-314 kJ/mol) < Na⁺ (-397 kJ/mol) < Li⁺ (-506 kJ/mol) < Ca²⁺ (-1,580 kJ/mol) < Mg²⁺ (-1,910 kJ/mol). Despite the subtle change in two divalent bentonites, the adsorption capacities of the three bentonites with monovalent exchangeable cations consistently increase with the increasing enthalpy of hydration, verifying the soundness of the proposed SWI model to probe the water sorption behavior of bentonite clays with diverse types of exchangeable cation.

As illustrated in Fig. 2(a), the non-expansive and expansive clays have very different hydration sequence, leading to some distinction in the water sorption behavior. Fig. 8 exhibits both the experimental and fitted isotherms for a series of clay samples prepared by mixing the nonswelling kaolinite and highly swelling bentonite at various mass ratios. Such a mixing can provide a series of clay samples with intermediate water adsorption capability proportionally distributed between the two end members. Will the proposed SWI model be able to predict the adsorption capability of

such mixtures? As shown in Fig. 8, the proposed SWI model gives a statistically perfect fitting ($R^2 = 1.00$) for the isotherm data of the mixtures, including the two end members.

Furthermore, the maximum water content retained by these soils at 0.95 RH ranges from 0.026 to 0.230 g/g, which increases almost linearly with the increasing dry-mass ratio of bentonite to kaolinite. The adsorption capacity varies from 0.01 to 0.15 g/g as the mixing ratio changes from 100% kaolinite to 100% bentonite. The adsorption capacities of the clay mixtures can also be

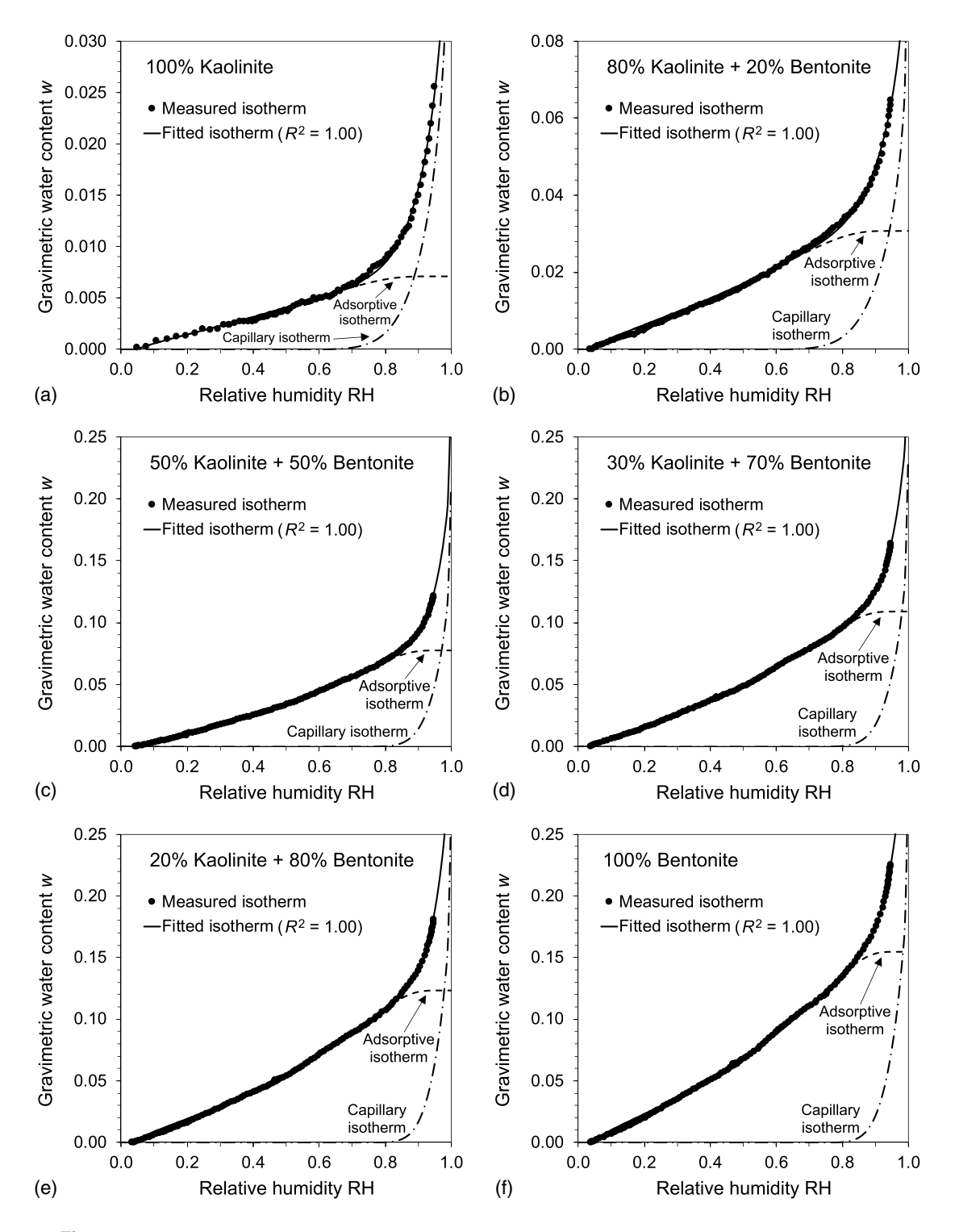


Fig. 8. Fitted isotherms and separated adsorptive and capillary isotherms for kaolinite-bentonite mixtures.

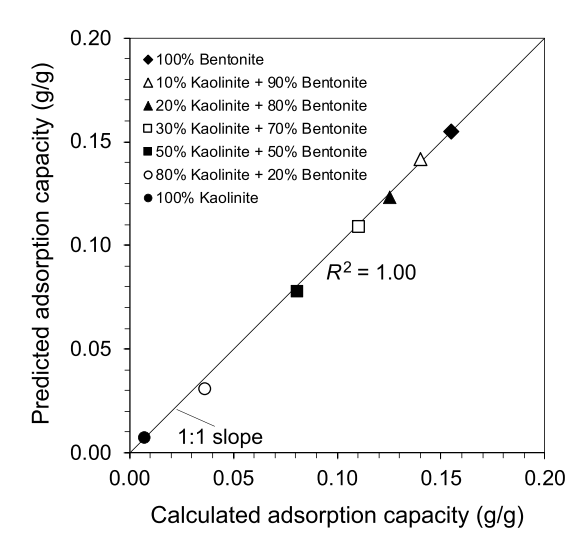


Fig. 9. Comparisons of the adsorption capacity predicted by the proposed SWI model and the end-member calculations for kaolinite-bentonite mixture.

calculated proportionately based on the adsorption capacities of the two end members (i.e., pure kaolinite and bentonite) and mass ratio. The adsorption capacities determined by the proposed SWI model compare very well ($R^2 = 1.00$) with that calculated from the two end members, as shown in Fig. 9, demonstrating the robustness of the proposed SWI model to identify a soil's adsorption capacity.

Comparison with Other SWI Models

The separation of adsorptive and capillary isotherms (Figs. 6–8) demonstrates that the transition process from adsorption to capillarity on a soil isotherm does not occur suddenly at one specific RH point but takes place gradually within a certain range of RH. The multilayer adsorption will continue after the onset of capillary condensation until it reaches the adsorption capacity, giving the transition regime a lower bound defined by the onset of capillary condensation and an upper bound defined by the completion of adsorption. However, neither the BET equation nor the A-BET equation functions in or beyond this transition regime (i.e., adsorbed film regime) due to their overlooking of capillarity. Fig. 10 facilitates such comparisons between the proposed SWI model, the A-BET equation, and the popular BET equation through the isotherms of six soils ranging from silt to swelling clay. As shown, these three SWI models have very different ranges suitable for representing the soil isotherm, and the proposed SWI model is observed to be the best one, showing $R^2 = 1.00$ for all six soils in Fig. 10. In general, the BET equation fits the isotherm well only at the RH less than approximately 0.3. Although the A-BET equation remarkably widens the range of BET, especially for swelling clay, by differentiating the adsorptions on external and internal clay surfaces (Lu and Zhang 2020), it is still far from the full coverage of RH. Isotherms determined from both BET and A-BET deviate from the experimental data prior to the completion of adsorption for most soils and are significantly overpredicted at the high RH range, owing to the absence of a capillary mechanism in these two models. The outperformance of the proposed SWI model in the transition and the subsequent capillary regimes demonstrates its capability to pinpoint the onset of capillary condensation, which further highlights the strength of the new model in representing soil water isotherms over the full range of RH.

Practical Implications

The proposed SWI opens a new horizon for understanding many fundamental properties of soil that are practically useful for geotechnical engineering, such as specific surface area, cation exchange capacity, water cavitation, soil freezing curve, soil water density, soil sorptive potential, Atterberg limits, elastic modulus, shear wave velocity, thermal conductivity, and hydraulic conductivity. For example, the capability of separating and quantifying a soil's adsorptive SWI and capillary SWI enables better characterizations of soil's intrinsic properties such as specific surface area (SSA) and pore-size distribution (PSD). The proposed adsorptive SWI provides a direct physical link between a soil's SSA and adsorptive water. While utilizing the Young-Laplace equation, the proposed capillary SWI can be directly used to determine a soil's PSD. This isotherm-based approach differs fundamentally from the mercury intrusion porosimetry (MIP) commonly used for PSD of fine-grained soil, because the PSD characterization from the SWI is attained on the basis of soil-water interactions whereas the MIP completely ignores the effect of soil swelling on PSD.

Historically, SWRC has been used to quantify PSD (e.g., Lowell and Shields 1984; Lu and Likos 2004), which can generalize the Kozeny–Carman (Kozeny 1927; Carman 1937) equation to formulate soil's hydraulic conductivity function (e.g., Marshall 1958; Jackson 1972). However, PSD in those formulations is only related to capillary pores through the Young–Laplace equation. Thus, hydraulic conductivity models based on the Kozeny–Carman equation are mostly suitable for capillary flow in coarse-grained soil. For fine-grained soil, recent studies have shown that adsorptive water is important in film flow (e.g., Tuller and Or 2001; Lebeau and Konrad 2010). However, to date, only a few SWRC or SWI models can quantify both capillary water and adsorptive water. The proposed SWI model is the first able to accurately separate SWI into capillary SWI and adsorptive SWI, opening a new window to better formulate hydraulic conductivity functions of fine-grained soils

To further illustrate the aforementioned practical implications, the authors exemplify the linkage between the adsorption capacity and the Atterberg limits. Considering that coarse-grained soil with little adsorptive ability has nondefinable Atterberg limits, Zhou and Lu (2021b) have recently suggested that the Atterberg limits can be correlated with the adsorption mechanism in fine-grained soil, specifically demonstrated by the relationship between the Atterberg limits (i.e., liquid limit, plastic limit, and plasticity index) and the adsorption capacity determined from the SWI modeling. Fig. 11 shows the plots of liquid limit, plastic limit, and plasticity index of 32 soils, for which Atterberg limits are available (Table 1), versus their corresponding adsorption capacities determined here based on the SWI modeling. Because the adsorption capacity can reflect soil's total SSA, which is one of the governing factors for Atterberg limits and plays a key role in resisting external loadings, i.e., rolling and shaking (Zhou and Lu 2021a), positive correlations are found in the three plots of Fig. 11 with the corresponding $R^2 = 0.84$, 0.52, and 0.82. Such correlations offer a potential pathway to classify soil based on soil physical properties.

Summary and Conclusions

SWI and SWRC are arguably the two most important soil constitutive relationships because they govern virtually all phenomena in soil such as flow, stress and deformation, and biological activities. These two functions can be connected via Kelvin's equation. SWI usually represents SWRC at medium to high suction range, i.e., ψ > 10³ kPa or RH < 0.99. Here, a closed-form SWI equation,

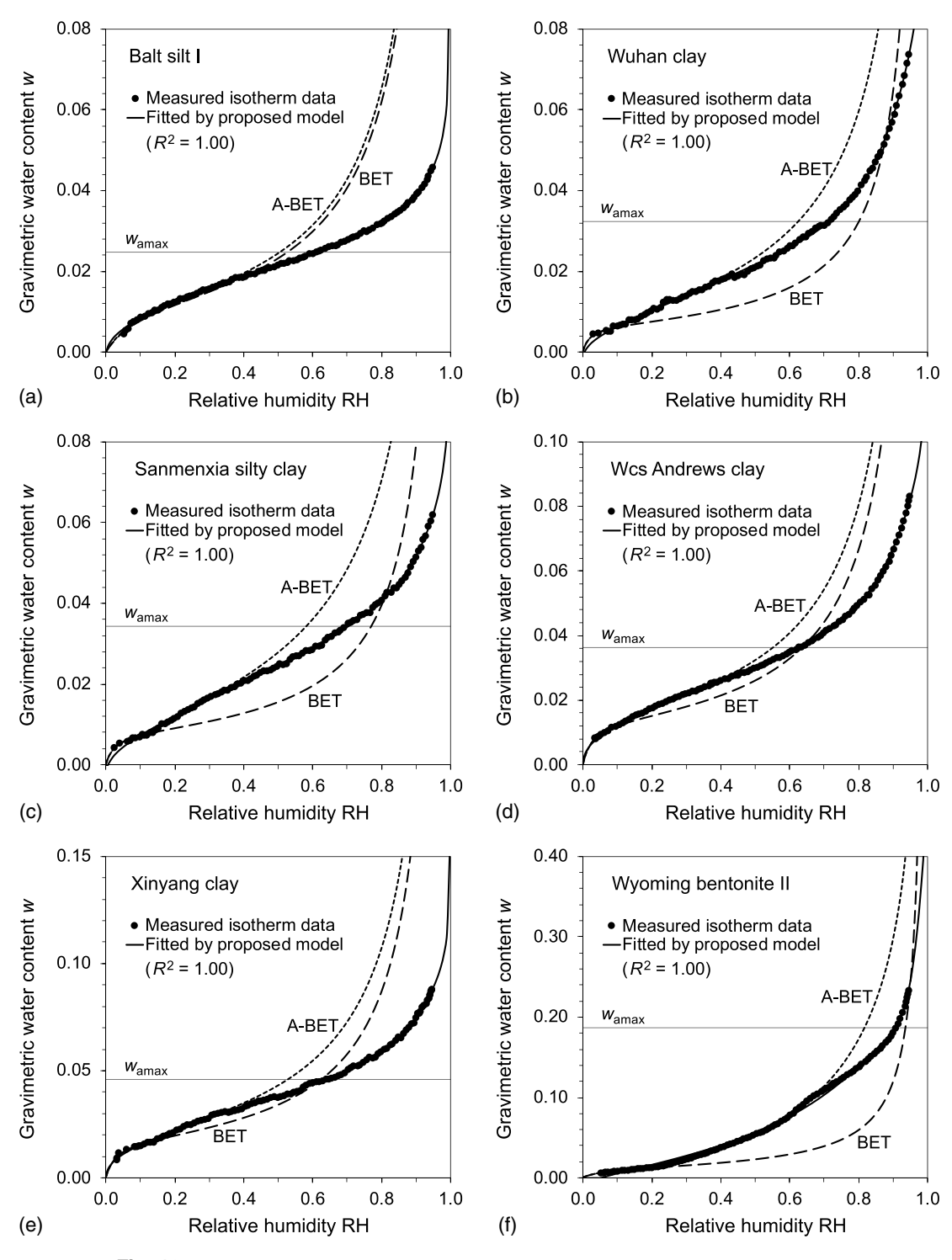


Fig. 10. Comparisons among the proposed model, BET equation, and A-BET equation.

recast from a generalized SWRC equation previously established based on physical water-retention mechanisms of adsorption and capillarity, is experimentally validated for its generality in representing SWI. The SWI equation can be decomposed into adsorptive and capillary isotherms, and the total water content under an equilibrium RH is a superposition of these two constituent parts. The newly proposed SWI model is fully defined by Eqs. (8), (12), and (13) with five model parameters; two for adsorptive water, namely the minimum relative humidity RH_{min} and adsorption capacity $w_{\rm amax}$; three for capillary water, namely the onset cavitation humidity ξ , extent of cavitation humidity ω , and pore-size distribution n.

A skew-normal distribution is adapted in the SWI model to better describe the cavitation/condensation phenomenon that occurred in capillary water.

Water sorption isotherms of 49 soils, covering all spectrum of soil types with plasticity index (PI) from 4% to 185%, specific surface area (SSA) from 21 up to 600 m²/g, and cation exchange capacity (CEC) from 0.4 up to 169.0 cmol/kg, are used to validate the generality of the SWI equation. The 49 soils include natural soils, cation-exchanged bentonites, and mixtures of kaolinite and bentonite. It is shown that the SWI equation can nearly perfectly represent the isotherms of sandy, silty, nonswelling, and swelling

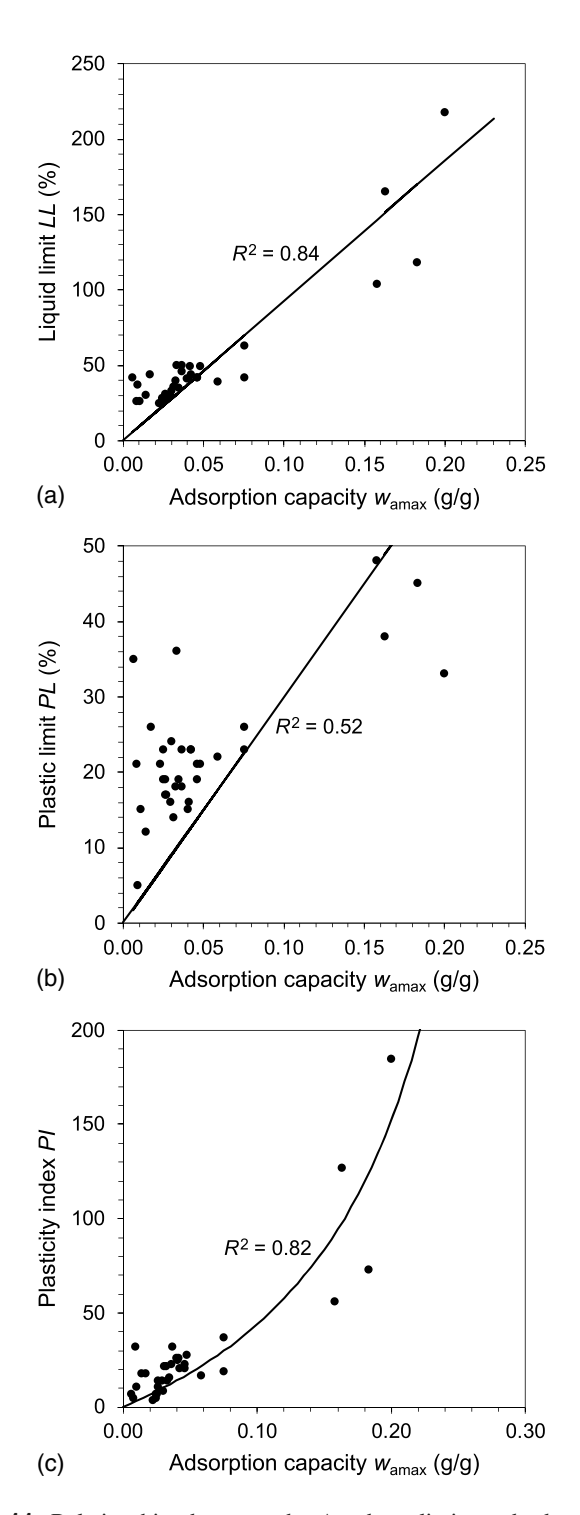


Fig. 11. Relationships between the Atterberg limits and adsorption capacity for 33 soils: (a) liquid limit versus adsorption capacity; (b) plastic limit versus adsorption capacity; and (c) plasticity index versus adsorption capacity.

soils with the coefficient of determination $R^2 \ge 0.99$, validating the generality of the SWI equation. Comparative analysis is also conducted for these soils by comparing the proposed SWI model with the other two existing SWI equations, namely, the BET equation and the augmented BET equation. It is demonstrated that the SWI equation is superior to the BET and A-BET equations in representing the measured soil water isotherm at the full range of RH, mainly due to the explicit inclusion of both adsorptive and capillary

water with clearly defined parameters based on soil water-retention mechanisms.

The adsorption capacities of soils identified by the new SWI model is comparable to the published data in the literature, showing a high correlation ($R^2=0.91$) with the results determined from the SWRC measurements by using the Lu's (2016) SWRC model. The demonstrated correlation between the adsorption capacity and the Atterberg limits further indicates that while the former is a controlling factor for the latter, other factors such as pore-size distribution, particle structure, and pore chemistry also play important roles in governing the Atterberg limits.

It is concluded that the proposed SWI model can accurately represent SWI, adsorptive SWI, and capillary SWI for all types of soil in the full relative humidity range. The proposed SWI model will open a new horizon for understanding many fundamental properties of soil practically useful for geotechnical engineering such as specific surface area, cation exchange capacity, water cavitation, soil freezing curve, soil water density, soil sorptive potential, Atterberg limits, elastic modulus, shear wave velocity, thermal conductivity, and hydraulic conductivity.

Data Availability Statement

All data, models, and code generated or used during the study appear in the published article.

Acknowledgments

This research is supported by the US National Science Foundation (NSF CMMI-1902045).

Notation

The following symbols are used in this paper:

a = air-entry suction;

c =constant of adsorption enthalpy;

 $c_{\text{m-ext}}$ = constant of adsorption enthalpy on external surface;

 $c_{\text{m-int}}$ = constant of adsorption enthalpy on internal surface;

 G_s = specific gravity;

M = adsorption strength;

n =parameter of pore-size distribution;

R = universal gas constant;

RH = relative humidity;

 RH_0 = initiation RH for internal adsorption;

 $RH_{min} = minimum RH;$

T = temperature;

 u_a = pore air pressure;

 $u_{\rm w}$ = pore water pressure;

 $v_{\rm w}$ = molar volume of water;

w = total water content;

 w_a = adsorptive water content;

 $w_{\text{amax}} = \text{adsorption capacity};$

 $w_{\rm c}$ = capillary water content;

 $w_{\rm m}$ = monolayer water content;

 $w_{\text{m-ext}}$ = monolayer water content on external surface;

 $w_{\text{m-int}}$ = monolayer water content on internal surface;

 $w_{\rm s}$ = saturated water content;

x = statistical distance to soil particle surface;

 α = shape parameter of a skew-normal distribution;

- σ_c = standard deviation of the cavitation CDF;
- σ_{RH} = standard deviation of a normal distribution;
- μ_{RH} = mean of a normal distribution;
 - ξ = RH onset for cavitation;
 - $\phi = \text{porosity};$
 - ψ = matric suction;
- ψ_c = mean cavitation suction;
- $\psi_{\rm max}$ = maximum suction;
- $\psi_{\rm sorp}$ = soil sorptive potential; and
 - $\omega = RH$ range for cavitation.

References

- Akin, I., and W. Likos. 2014. "Specific surface area of clay using water vapor and EGME sorption methods." *Geotech. Testing J.* 37 (6): 1016–1027. https://doi.org/10.1520/GTJ20140064.
- Akin, I., and W. Likos. 2016. "Single-point and multi-point water-sorption methods for specific surface areas of clay." *Geotech. Test. J.* 39 (2): 291–300. https://doi.org/10.1520/GTJ20150117.
- ASTM. 2017. Standard practice for classification of soils for engineering purposes (unified soil classification system). ASTM D2487-17. West Conshohocken, PA: ASTM.
- Bohn, H. L., B. L. McNeal, and G. A. O'Connor. 2001. *Soil chemistry*. New York: Wiley.
- Brunauer, S., P. H. Emmett, and E. Teller. 1938. "Adsorption of gases in multimolecular layers." *J. Am. Chem. Soc.* 60 (2): 309–319. https://doi.org/10.1021/ja01269a023.
- Carman, P. C. 1937. "Fluid flow through granular beds." *Trans. Inst. Chem. Eng.*, 15: 150–166. London: Institution of Chemical Engineers.
- Caupin, F., and E. Herbert. 2006. "Cavitation in water: A review." C.R. Phys. 7 (9): 1000–1017. https://doi.org/10.1016/j.crhy.2006.10.015.
- Chen, F. H. 1988. Foundations on expansive soils. New York: Elsevier.
 Debenedetti, P. G. 1996. Metastable liquids: Concepts and principles.
 Princeton, NJ: Princeton University Press.
- Derjaguin, B. V., N. V. Churaev, and V. M. Muller. 1987. *Surface forces*. New York: Plenum Publishing.
- Dong, Y., and N. Lu. 2016. "Correlation between small-strain shear modulus and suction stress in capillary regime under zero total stress conditions." *J. Geotech. Geoenviron. Eng.* 142 (11): 4016056. https://doi.org/10.1061/(ASCE)GT.1943-5606.0001531.
- Dong, Y., and N. Lu. 2020. "Measurement of suction stress and soil deformation at high suction range." *Geotech. Test. J.* 44 (2): 308–322. https://doi.org/10.1520/GTJ20190357.
- Du, J., A. Zhou, X. Lin, Y. Bu, and J. Kodikara. 2021. "Prediction of swelling pressure of expansive soil using an improved molecular dynamics approach combining diffuse double layer theory." *Appl. Clay Sci.* 203 (Mar): 105998. https://doi.org/10.1016/j.clay.2021.105998.
- Elzhov, T. V., K. M. Mullen, A.-N. Spiess, and B. Bolker. 2016. "R interface to the Levenberg-Marquardt nonlinear least-squares algorithm found in MINPACK, plus support for bounds." Comprehensive R Archive Network. Accessed November 20, 2016. https://cran.r-project.org/web/packages/minpack.lm/minpack.lm.pdf.
- Fredlund, D. G., and A. Xing. 1994. "Equations for the soil-water characteristic curve." *Can. Geotech. J.* 31 (4): 521–532. https://doi.org/10.1139/t94-061.
- Frydman, S., and R. Baker. 2009. "Theoretical soil-water characteristic curves based on adsorption, cavitation, and a double porosity model." *Int. J. Geomech.* 9 (6): 250–257. https://doi.org/10.1061/(ASCE)1532 -3641(2009)9:6(250).
- Herbert, E., S. Balibar, and F. Caupin. 2006. "Cavitation pressure in water." *Phys. Rev. E* 74 (4): 41603. https://doi.org/10.1103/PhysRevE.74
- Hillel, D. 1998. Environmental soil physics. San Diego: Academic Press. Iwata, S., T. Tabuchi, and B. P. Warkentin. 1995. Soil-water interactions: Mechanisms and applications. New York: Marcel Dekker.

- Jackson, R. D. 1972. "On the calculation of hydraulic conductivity." Soil Sci. Soc. Am. J. 36 (2): 380–382. https://doi.org/10.2136/sssaj1972 .03615995003600020047x.
- Jensen, D. K., M. Tuller, L. W. de Jonge, E. Arthur, and P. Moldrup. 2015. "A new two-stage approach to predicting the soil water characteristic from saturation to oven-dryness." *J. Hydrol.* 521 (Feb): 498–507. https://doi.org/10.1016/j.jhydrol.2014.12.018.
- Keren, R., and I. Shainberg. 1979. "Water vapor isotherms and heat of immersion of Na/Ca-montmorillonite systems—II: Mixed systems." Clays Clay Miner. 27 (2): 145–151. https://doi.org/10.1346/CCMN.1979 0270212.
- Khorshidi, M., and N. Lu. 2017a. "Intrinsic relation between soil water retention and cation exchange capacity." *J. Geotech. Geoenviron. Eng.* 143 (4): 4016119. https://doi.org/10.1061/(ASCE)GT.1943-5606.0001633.
- Khorshidi, M., and N. Lu. 2017b. "Determination of cation exchange capacity from soil water retention curve." J. Eng. Mech. 143 (6): 4017023. https://doi.org/10.1061/(ASCE)EM.1943-7889.0001220.
- Khorshidi, M., N. Lu, I. D. Akin, and W. J. Likos. 2017. "Intrinsic relationship between specific surface area and soil water retention." *J. Geotech. Geoenviron. Eng.* 143 (1): 4016078. https://doi.org/10.1061/(ASCE) GT.1943-5606.0001572.
- Khorshidi, M., N. Lu, and A. Khorshidi. 2016. "Intrinsic relationship between matric potential and cation hydration." *Vadose Zone J.* 15 (11): 1–12. https://doi.org/10.2136/vzj2016.01.0001.
- Koopmans, R. W. R., and R. D. Miller. 1966. "Soil freezing and soil water characteristic curves." *Soil Sci. Soc. Am. J.* 30 (6): 680–685. https://doi .org/10.2136/sssaj1966.0361599500300060011x.
- Kozeny, J. 1927. "Ueber kapillare leitung des wassers im boden." Sitzungsberichte Wiener Akademie 136 (2): 271–306.
- Kurylyk, B. L., and K. Watanabe. 2013. "The mathematical representation of freezing and thawing processes in variably-saturated, nondeformable soils." Adv. Water Resour. 60 (2): 160–177. https://doi.org/10.1016/j .advwatres.2013.07.016.
- Lebeau, M., and J.-M. Konrad. 2010. "A new capillary and thin film flow model for predicting the hydraulic conductivity of unsaturated porous media." *Water Resour. Res.* 46 (12): W12554. https://doi.org/10.1029/2010WR009092
- Likos, W., N. Lu, and W. Wenszel. 2011. "Performance of a dynamic dew point method for moisture isotherms of clays." *Geotech. Test. J.* 34 (4): 373–382. https://doi.org/10.1520/GTJ102901.
- Likos, W. J. 2008. "Vapor adsorption index for expansive soil classification." J. Geotech. Geoenviron. Eng. 134 (7): 1005–1009. https://doi.org/10.1061/(ASCE)1090-0241(2008)134:7(1005).
- Likos, W. J., and N. Lu. 2002. "Water vapor sorption behavior of smectite-kaolinite mixtures." Clays Clay Miner. 50 (5): 553–561. https://doi.org/10.1346/000986002320679297.
- Lowell, S., and J. E. Shields. 1984. *Powder surface area DNA porosity*. New York: Chapman and Hall.
- Lu, N. 2016. "Generalized soil water retention equation for adsorption and capillarity." J. Geotech. Geoenviron. Eng. 142 (10): 4016051. https:// doi.org/10.1061/(ASCE)GT.1943-5606.0001524.
- Lu, N. 2019a. "Linking soil water adsorption to geotechnical engineering properties." In *Geotechnical fundamentals for addressing new world challenges*, edited by N. Lu and J. K. Mitchell, 93–139. Berlin: Springer.
- Lu, N. 2019b. "Revisiting axis translation for unsaturated soil testing." J. Geotech. Geoenviron. Eng. 145 (7): 2819001.
- Lu, N. 2020. "Unsaturated soil mechanics: Fundamental challenges, break-throughs, and opportunities." J. Geotech. Geoenviron. Eng. 146 (5): 2520001. https://doi.org/10.1061/(ASCE)GT.1943-5606.0002233.
- Lu, N., and M. Khorshidi. 2015. "Mechanisms for soil-water retention and hysteresis at high suction range." J. Geotech. Geoenviron. Eng. 141 (8): 4015032. https://doi.org/10.1061/(ASCE)GT.1943-5606.0001325.
- Lu, N., and W. J. Likos. 2004. *Unsaturated soil mechanics*. New York: Wiley
- Lu, N., and C. Zhang. 2019. "Soil sorptive potential: Concept, theory, and verification." J. Geotech. Geoenviron. Eng. 145 (4): 4019006. https:// doi.org/10.1061/(ASCE)GT.1943-5606.0002025.

- Lu, N., and C. Zhang. 2020. "Separating external and internal surface areas of soil particles." *J. Geotech. Geoenviron. Eng.* 146 (2): 4019126. https://doi.org/10.1061/(ASCE)GT.1943-5606.0002198.
- Marshall, T. J. 1958. "A relation between permeability and size distribution of pores." *J. Soil Sci.* 9 (1): 1–8. https://doi.org/10.1111/j.1365-2389 .1958.tb01892.x.
- McKeen, R. G. 1992. "A model for predicting expansive soil behavior." In Vol. 1 of *Proc.*, 7th Int. Conf. on Expansive Soils, 1–6. London; Lubbock, TX: International Society of Soil Mechanics and Foundation Engineering; Texas Tech Univ.
- McQueen, I. S., and R. F. Miller. 1974. "Approximating soil moisture characteristics from limited data: Empirical evidence and tentative model." *Water Resour. Res.* 10 (3): 521–527. https://doi.org/10.1029 /WR010i003p00521.
- Montes-H, G., J. Duplay, L. Martinez, Y. Geraud, and B. Rousset-Tournier. 2003. "Influence of interlayer cations on the water sorption and swelling–shrinkage of MX80 bentonite." *Appl. Clay Sci.* 23 (5): 309–321. https://doi.org/10.1016/S0169-1317(03)00130-3.
- Mooney, R. W., A. G. Keenan, and L. A. Wood. 1952. "Adsorption of water vapor by montmorillonite. II. Effect of exchangeable ions and lattice swelling as measured by X-ray diffraction." *J. Am. Chem. Soc.* 74 (6): 1371–1374. https://doi.org/10.1021/ja01126a002.
- Mualem, Y. 1976. "A new model for predicting the hydraulic conductivity of unsaturated porous media." *Water Resour. Res.* 12 (3): 513–522. https://doi.org/10.1029/WR012i003p00513.
- Or, D., and M. Tuller. 2002. "Cavitation during desaturation of porous media under tension." *Water Resour. Res.* 38 (5): 1–19. https://doi.org/10.1029/2001WR000282.
- Or, D., M. Tuller, and J. M. Wraith. 2005. "Soil water potential." In Encyclopedia of soils in the environment, 1st ed., edited by D. Hillel, 270–277. Cambridge, MA: Academic Press.
- Osman, K. T. 2013. *Soils: Principles, properties and management*. Berlin: Springer.
- Pomonis, P. J., D. E. Petrakis, A. K. Ladavos, K. M. Kolonia, G. S. Armatas, S. D. Sklari, P. C. Dragani, A. Zarlaha, V. N. Stathopoulos, and A. T. Sdoukos. 2004. "A novel method for estimating the C-values of the BET equation in the whole range 0 < P/Po > 1 using a Scatchard-type treatment of it." *Microporous Mesoporous Mater*. 69 (1): 97–107. https://doi.org/10.1016/j.micromeso.2004.01.009.
- Revil, A., and N. Lu. 2013. "Unified water isotherms for clayey porous materials." Water Resour. Res. 49 (9): 5685–5699. https://doi.org/10 .1002/wrcr.20426.

- Schanz, T., and S. Tripathy. 2009. "Swelling pressure of a divalent-rich bentonite: Diffuse double-layer theory revisited." *Water Resour. Res.* 45 (5): W00C12. https://doi.org/10.1029/2007WR006495.
- Tuller, M., and D. Or. 2001. "Hydraulic conductivity of variably saturated porous media: Film and corner flow in angular pore space." Water Resour. Res. 37 (5): 1257–1276. https://doi.org/10.1029/2000WR900328.
- Tuller, M., and D. Or. 2005. "Water films and scaling of soil characteristic curves at low water contents." *Water Resour. Res.* 41 (9): W09403. https://doi.org/10.1029/2005WR004142.
- van Genuchten, M. T. 1980. "A closed-form equation for predicting the hydraulic conductivity of unsaturated soils." *Soil Sci. Soc. Am. J.* 44 (5): 892–898. https://doi.org/10.2136/sssaj1980.03615995004400050002x.
- Villar, M. V., and A. Lloret. 2008. "Influence of dry density and water content on the swelling of a compacted bentonite." *Appl. Clay Sci.* 39 (1): 38–49. https://doi.org/10.1016/j.clay.2007.04.007.
- Yamanaka, S., P. B. Malla, and S. Komarneni. 1990. "Water adsorption properties of alumina pillared clay." *J. Colloid Interface Sci.* 134 (1): 51–58. https://doi.org/10.1016/0021-9797(90)90250-R.
- Zhang, C., Y. Dong, and Z. Liu. 2017. "Lowest matric potential in quartz: Metadynamics evidence." *Geophys. Res. Lett.* 44 (4): 1706–1713. https://doi.org/10.1002/2016GL071928.
- Zhang, C., and N. Lu. 2018. "What is the range of soil water density? Critical reviews with a unified model." *Rev. Geophys.* 56 (3): 532–562. https://doi.org/10.1029/2018RG000597.
- Zhang, C., and N. Lu. 2019a. "Augmented Brunauer–Emmett–Teller equation for water adsorption on soils." *Vadose Zone J.* 18 (1): 190011.
- Zhang, C., and N. Lu. 2019b. "Unitary definition of matric suction." J. Geotech. Geoenviron. Eng. 145 (2): 2818004. https://doi.org/10.1061/(ASCE)GT.1943-5606.0002004.
- Zhang, C., and N. Lu. 2020. "Soil sorptive potential: Its determination and predicting soil water density." J. Geotech. Geoenviron. Eng. 146 (1): 4019118. https://doi.org/10.1061/(ASCE)GT.1943-5606.0002188.
- Zhou, B., and N. Lu. 2021a. "Assessments of water sorption methods to determine soil's specific surface area." J. Geotech. Geoenviron. Eng. 147 (8): 4021066. https://doi.org/10.1061/(ASCE)GT.1943-5606 .0002579.
- Zhou, B., and N. Lu. 2021b. "Correlation between Atterberg limits and soil adsorptive water." *J. Geotech. Geoenviron. Eng.* 147 (2): 4020162. https://doi.org/10.1061/(ASCE)GT.1943-5606.0002463.